Aalborg Universitet

AALBORG UNIVERSITY
DENMARK

Millimeter Wave Multi-user Performance Evaluation Based on Measured Channels with Virtual Antenna Array Channel Sounder

Mbugua, Allan Wainaina; Fan, Wei; Ji, Yilin; Pedersen, Gert F.

Millimeter Wave Multi-user Performance Evaluation Based on Measured Channels with Virtual Antenna Array Channel Sounder

Allan Wainaina Mbugua, Wei Fan, Yilin Ji and Gert Frølund Pedersen

Abstract—Virtual antenna arrays are versatile and cost-effective tools for millimeter-wave (mm-wave) channel characterization. Massive sampling of the channel in space with virtual antenna arrays enable high spatial resolution in channel sounding. In this paper, a uniform cubic array (UCuA) is used with a Vector Network Analyzer (VNA) to characterize an indoor propagation channel. The power angle delay profile (PADP) under line-of-sight (LOS) and obstructed-line-of-sight (OLOS) scenarios are then extracted from the measurement data. The analysis is extended to a multi-user scenario using a virtual uniform rectangular array (URA) which acts as the base station (BS) and with users under LOS and OLOS conditions. Results show interference suppression with zero-forcing beamforming (ZF-BF) performs well even in critical multi-user scenarios based on the measured channels, i.e. a scenario with closely spaced users in LOS conditions, and a scenario with a strong interfering user and a weak desired user.

Index Terms—5G, channel sounding, millimeter wave, radio propagation, virtual antenna array.

I. INTRODUCTION

The prospects of achieving 1000 times (1000x) fold data rate increase for the fifth generation (5G) mobile network have spurred a lot of interest in mm-wave bands where a large contiguous bandwidth is available [1]. The small wavelength at mm-wave frequencies allow the implementation of compact antenna arrays and thus the path loss suffered at these bands can be mitigated by the antenna array gain [2], [3].

The need for accurate characterization of mm-wave band channels has led to intensive measurement campaigns in recent years. The most popular channel sounding techniques employed are VNA based virtual-array systems and sliding correlation based systems. Sliding correlation systems employ a pseudo-random noise (PN) sequence known both to the transmitter (Tx) and receiver (Rx). This technique allows tether free operation of the Tx and Rx, but on the other hand increases the complexity of clock synchronization [4], [5].

The VNA is a relatively cheap tool for performing ultra-wideband (UWB) channel sounding. This is accomplished easily by performing a frequency sweep over the band of interest. The Tx and Rx are connected by cable to the VNA, from where the clock synchronization is handled thus reducing system complexity. However, the cable connection of both the Tx and Rx to the VNA results in a limitation of the

Allan Wainaina Mbugua, Wei Fan, Yilin Ji and Gert Frølund Pedersen are with the Antennas, Propagation and Millimetre-Wave Systems Section, Department of Electronic Systems, Faculty of Engineering and Science, Aalborg University, Aalborg 9220, Denmark (e-mail: awm,wfa,yilin,gfp@es.aau.dk).

measurement distance especially at mm-wave bands due to a high signal loss in the cables. The measurement distance can be increased by using optical cables [6] or downconverting the signal at the Rx to a lower frequency to reduce the signal loss in the cables [7].

Channel directional information can be obtained with the VNA sounding technique by mechanically steering horn antennas or electrical steering with virtual antenna arrays. The drawback of using horn antennas is that the spatial resolution is limited by the beamwidth of the antenna [8]. Virtual antenna arrays, on the other hand, are easy to implement and have no mutual coupling [9]. The drawback of virtual antenna arrays is that the channel has to be kept static. Thus this method is not applicable when Doppler information is required or in dynamic propagation environments. Moreover, the measurement time can scale up to several hours when the number of virtual antenna array elements is massive.

The flexibility of virtual arrays means that arbitrary arrays can be easily implemented. This reduces the cost of channel measurement equipment and facilitates practical evaluation of state-of-the-art techniques such as massive multiple-input multiple-output (MIMO) at mm-wave [3]. In [8], [10], a virtual uniform circular array (UCA) is used since the beam pattern is uniform in the azimuth plane. However, the UCA suffers joint sidelobes in delay and angle domain when using the Bartlett beamformer. The sidelobes problem is mitigated by the use of a frequency invariant beamforming algorithm in [11]. Although this algorithm reduces the sidelobes, the sidelobes of the LOS component are not suppressed sufficiently. A virtual UCuA enables massive sampling of the channel in the spatial domain resulting in high three-dimensional (3D) directional resolution. In [12], [13], the UCuA is shown to provide unambiguous directional information with significant sidelobes suppression when using the Bartlett beamformer.

5G is expected to offer great service even in crowded scenarios [14], [15]. These propagation scenarios are challenging due to channel similarities for the users. The spatial separation of users in such scenarios becomes critical for interference-free communication. Massive MIMO can be leveraged in these situations to mitigate the interference among the users. The attractive features of massive MIMO at mm-wave bands, like the near optimal performance of sub-optimal linear precoding schemes have been mainly investigated in theoretic analysis via numerical analysis which clearly lacks the support of practical channel sounding measurements. To bring this technique from theory to practice we must ask

to what extent the theoretical analysis can be maintained in realistic propagation environments. Though the theoretical analysis is mature few measurement campaigns have been reported for mm-wave bands. The measurements reported in literature are mainly for sub-6 GHz bands [16], [17]. However, there are distinct differences in the mm-wave bands and the sub-6 GHz bands, with the former exhibiting channel sparsity and directivity [8], [18]. This work bridges the gap between the theoretical analysis and real-world performance of zero-forcing (ZF) precoding, with a focus on critical multi-user scenarios.

The spatial-temporal characteristic of the channel is first obtained using a VNA based virtual UCuA. Two critical multi-user scenarios are then investigated with the aforementioned channel sounding method and a virtual URA. In the first case the users are closely spaced with a dominant LOS component and in the second case, the targeted user is weak with a strong interferer, which mimics the case where cell-edge users suffer interference from users close to the BS.

The rest of the paper is organised as follows: In section II the measurement system and the measurement scenario are presented. Section III outlines the classical beamforming ZF-BF and algorithms used in the analysis of the data and the results are then demonstrated in section IV. Finally, section V concludes the paper.

Notation: $(\cdot)^{\dagger}$ is the pseudo-inverse, $(\cdot)^{H}$ is the conjugate transpose (Hermitian), $(\cdot)^{-1}$ inverse. $(\cdot)^{\perp}$ is the orthogonal complement. $\|\cdot\|_{F}$ is the Frobenius norm. Matrices are denoted by boldface uppercase letters whereas vectors are denoted by lowercase boldface letters. λ denote the wavelength.

II. MEASUREMENT SETUP

A. Measurement System

The VNA utilized in the measurement campaign is *Keysight PNA N5227A*. The measurement was carried out at a center frequency of 28 GHz with 1500 frequency points and a bandwidth of 4 GHz. Thus a delay resolution of 0.25 ns was obtained. The VNA intermediate frequency (IF) bandwidth was set to 0.5 kHz so as to increase the dynamic range of the system at a cost of increased sweep time. With these VNA settings, a frequency sweep time of 2.89 s was obtained. The Tx power at port 1 of the VNA is set to 11 dBm.

Precision linear positioning stages *(Physik Instrumente PI M-415.DGX)* are used to create virtual antenna arrays used in the measurement campaign by moving the Tx antenna to predefined positions as shown in Fig. 1. This was automated with Python PyVisa instrument control library. The length of the linear positioning stages is 15 cm for the X and Y axes, and 5 cm for the Z axis.

The Tx antenna is a vertically polarized biconical antenna with a frequency range of 1.5 GHz to 41 GHz [19]. The Rx antennas *(AINFO-SZ-2003000/P)* are also vertically polarized biconical antennas with a frequency range of 2 GHz to 30 GHz. The antennas have an omnidirectional pattern in the azimuth plane. The antennas are placed at a height of 1.47 m above the floor which is approximately half the distance between the floor and the ceiling.
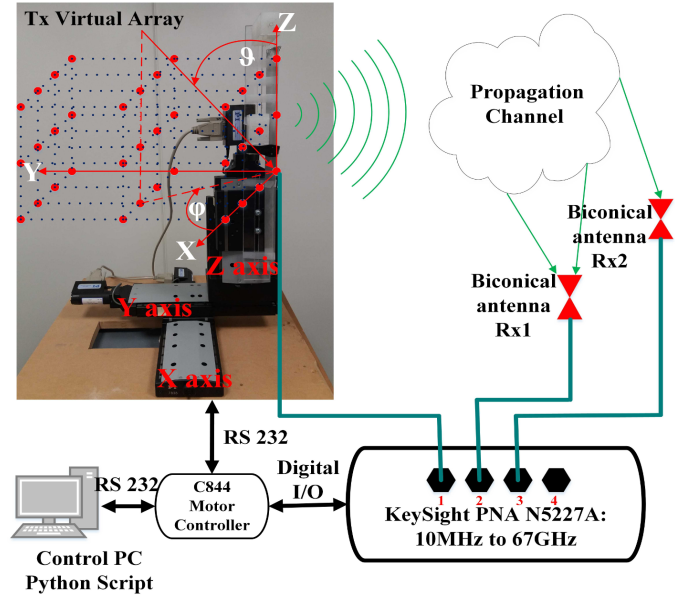

Fig. 1: Measurement Setup.

The VNA was given a warm-up time of at least 30 minutes, then a back to back calibration procedure is carried out before conducting measurements. The virtual antenna array inter-element distance d was set to 0.414λ at 30 GHz to avoid grating lobes in the array pattern. Massive sampling in space is carried out and a total of $(30 \times 30 \times 10)$ points are recorded for the UCuA with the origin of the coordinate system $(0, 0, 0)$. In the case of the URA, a total of (30×10) points are recorded. This resulted in a virtual UCuA of electrical length $12\lambda \times 12\lambda \times 4\lambda$ at 30 GHz $(0.414\lambda \times 29 = 12\lambda)$ and a virtual URA of electrical length $12\lambda \times 4\lambda$ at 30 GHz. During this time period, the environment is kept static. The measurement setup is illustrated in Fig. 1.

B. Measurement Scenario

The measurement campaign was carried out in a 36 m² kitchen/meeting room as shown in Fig. 2 and Fig. 3 where most of the furniture had been removed. This room was chosen since a static environment could be maintained for the entire duration of the measurement campaign. The two walls where the windows are located are made of concrete while the other two walls are made of plasterboard. A metallic whiteboard is fixed on the concrete wall behind the antenna Rx1 in Fig. 2a.

1) Channel sounding: For channel sounding analysis the UCuA is used where one Rx antenna is placed in LOS and the second Rx antenna is placed in OLOS. The OLOS scenario is created by placing a 0.74 m² copper plate raised 1 m above the floor using an aluminum ladder to block the direct paths between the Tx and one Rx antenna. The two cases are illustrated in Fig. 2.

2) Multi-user Scenario: For the multi-user scenario, the URA is used instead of the UCuA due to time constraint. The URA which mimics a BS is located along the YZ plane. Two
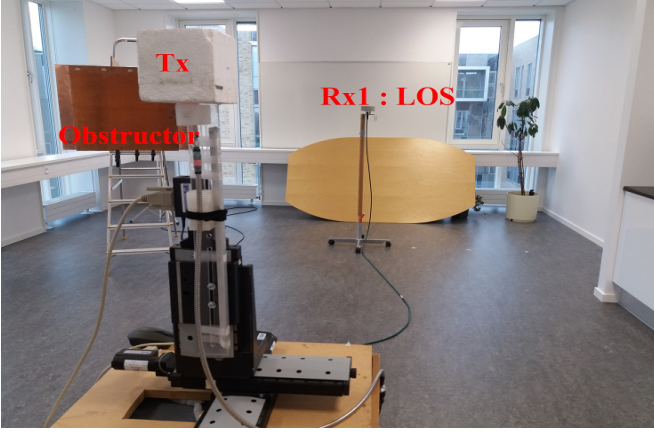
(a) View from the Tx antenna.

(b) View from the Rx antennas.

Fig. 2: Measurement scenario photos. Rx1 and Rx2 are the antennas for the LOS and OLOS respectively.

cases are investigated, with the first case having one user in LOS conditions while the second user is in OLOS conditions as shown in Fig. 2. The second case is where the two users are both in LOS conditions but with different user spacing as shown in Fig. 3. The two users are denoted as mobile station (MS)1 and MS2 respectively. MS1 is always fixed at location A while MS2 is placed at each of the four locations (A, B, C, and D). The four locations are in a line parallel to the URA. The MS separation distance is increased progressively by 0.5 m (50λ at 30 GHz) from location A to D.

III. SPATIAL-TEMPORAL CHANNEL CHARACTERISTIC

The spatial-temporal characteristic of the channel is obtained using the classical beamforming algorithm which is chosen for its simplicity and robustness.
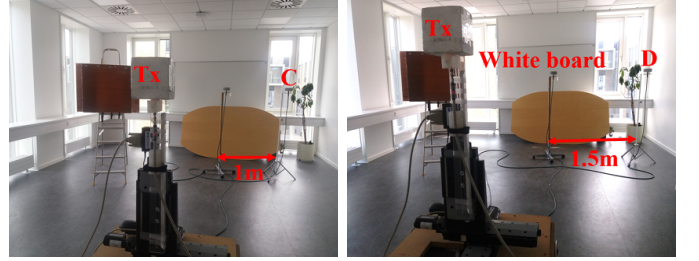
A. System Model

Let the UCuA be made of L elements in the x-axis M in the y-axis and N in the z-axis with an inter-element distance of 0.414λ for all the axes. The origin of the coordinate system $(0, 0, 0)$ is taken as the reference.

The channel frequency response at the origin $H(f)$ can thus be obtained as:

(a) Location A.

(b) Location B.

(c) Location C.

(d) Location D.

Fig. 3: Measurement scenario photos for the multi-user scenario in LOS conditions. One Rx antenna is fixed at location A, while the second Rx antenna is moved to the four locations(A,B,C and D).

$$H(f) = \sum_{k=0}^{K-1} \alpha_k e^{-j2\pi f \tau_k} \tag{1}$$

where τ_k and α_k are the delay of the *k-th* path and the complex amplitude respectively.

The time taken by the *k-th* plane wave whose angle of arrival (AOA) is (θ_k, φ_k) to reach the element l, m, n with respect to the origin is given as:

$$\tau_{k_{l,m,n}}(\theta_k, \varphi_k) = -\frac{\mathbf{p}_{l,m,n} \cdot \hat{\mathbf{u}}(\theta_k, \varphi_k)}{c} \tag{2}$$

Here we have defined $\mathbf{p}_{l,m,n}$ as the position vector of the element l, m, n which is given as:

$$\mathbf{p}_{l,m,n} = \begin{bmatrix} d(l-1) \\ d(m-1) \\ d(n-1) \end{bmatrix} \tag{3}$$

$\hat{\mathbf{u}}(\theta_k, \varphi_k)$ - the unit vector in the direction (θ_k, φ_k) which is defined as:

$$\hat{\mathbf{u}}(\theta_k, \varphi_k) = \begin{bmatrix} \sin(\theta_k)\cos(\varphi_k) \\ \sin(\theta_k)\sin(\varphi_k) \\ \cos(\theta_k) \end{bmatrix} \tag{4}$$

where $(\cdot)$ is the dot product, c is the speed of light and d is the array inter-element distance.

The frequency response of each element $H_{l,m,n}(f)$ is simply $H(f)$ shifted in phase [8] as:

$$H_{l,m,n}(f) = \sum_{k=0}^{K-1} \alpha_k e^{-j2\pi f (\tau_k + \tau_{k_{l,m,n}})} \tag{5}$$

The l, m, n element frequency response can be aligned to the reference element using the respective complex weight $w_{l,m,n}$, and thus the array frequency response is obtained as:

$$\mathbf{H}(f, \theta, \varphi) = \frac{1}{L}\frac{1}{M}\frac{1}{N} \sum_{l=0}^{L-1} \sum_{m=0}^{M-1} \sum_{n=0}^{N-1} w_{l,m,n} H_{l,m,n}(f) \quad (6)$$

The complex weight for the l, m, n element, $w_{l,m,n}$ is defined as:

$$w_{l,m,n} = e^{\frac{-j2\pi}{\lambda}\mathbf{p}_{l,m,n}\cdot\hat{\mathbf{u}}(\theta_k,\varphi_k)} \quad (7)$$

Finally, the spatial-temporal response is obtained by taking the inverse fast Fourier transform (IFFT) of the array frequency response.

$$\mathbf{h}(\tau, \theta, \varphi) = \sum_{n=0}^{N-1} \mathbf{H}(f_n, \theta, \varphi)e^{j2\pi f_n\tau} \quad (8)$$

where f_n is the n-th frequency bin.

The spatial-temporal for the URA can be obtained in a similar way by considering M elements in the y-axis and N elements in the z-axis and modifying eq. (6).

B. Multi-User Propagation Channel

The multi-user propagation channel in this analysis is modeled as a single-cell, where the BS consists of K antennas serving M single-antenna users. Considering a single frequency which in this analysis is the center frequency, the channel matrix $\mathbf{H} \in \mathbb{C}^{M \times K}$ can be represented as:

$$\mathbf{H} = \begin{bmatrix} h_{11} & \dots & h_{1K} \\ \vdots & \ddots & \vdots \\ h_{M1} & \dots & h_{MK} \end{bmatrix} = \begin{bmatrix} \mathbf{h}_1 \\ \vdots \\ \mathbf{h}_M \end{bmatrix} \quad (9)$$

In this analysis, ZF precoding is employed at the BS downlink. The ZF precoding scheme basically works on the principle of channel inversion, to null the interfering user, that is, the interfering user is projected onto the orthogonal complement of the desired user [20]. The shortcomings of ZF are manifested when user-channels are non-orthogonal. Assuming that at the BS, we have a total transmit power constraint, then there will be a trade-off between the achievable nulling of the interference and power allocated to the users [21], [22]. The orthogonal projection of user m denoted as $\mathbf{\Pi}_m$ is given as:

$$\mathbf{\Pi}_m = \mathbf{h}_m^{\dagger}\mathbf{h}_m \quad (10)$$

$\mathbf{h}_m^{\dagger}$ is the pseudo-inverse of the user m channel $\mathbf{h}_m$ which is given as:

$$\mathbf{h}_m^{\dagger} = \mathbf{h}_m^H(\mathbf{h}_m\mathbf{h}_m^H)^{-1}. \quad (11)$$

The interference from user j can be nulled by projecting its orthogonal projection $\mathbf{\Pi}_j$ onto the null space of user m:

$$\mathbf{\Pi}_m^{\perp} = \mathbf{I} - \sum_{j=1,j\neq m}^{M} \mathbf{\Pi}_j \quad (12)$$

where $\mathbf{I}$ is a $K \times K$ identity matrix and $j \in [1, \cdots, M] \; \forall j \neq m$ is the interfering user. The ZF-BF vector for user m, $\mathbf{w}_m \in \mathbb{C}^{K \times 1}$ can be generated from $\mathbf{\Pi}_m^{\perp}$ as:

$$\mathbf{w}_m = \frac{\mathbf{\Pi}_m^{\perp H}\mathbf{h}_m^H}{\left\|\mathbf{\Pi}_m^{\perp H}\mathbf{h}_m^H\right\|_F} \quad (13)$$

The power azimuth profile (PAP) with ZF-BF can then be obtained as in eq. (6) and substituting the antenna element frequency response with the corresponding channel coefficient from eq. (13).

IV. RESULTS

A. Channel Directional Analysis

In this analysis, a dynamic range of 30 dB is considered for the UCuA and 25 dB for the URA since the URA has a higher sidelobe level compared to the UCuA as was also observed in [12].

The virtual UCuA provides high resolution directional information with a low sidelobe level as shown in Fig. 4 and Fig. 5 for the LOS and OLOS scenario respectively. In both scenarios, the mm-wave channel is sparse and characterized by a few multipath components (MPC)s which is also observed in [8] at 28 GHz and in [12] at 60 GHz. The MPCs are due to first order and second order reflections. A power difference of 9 dB is observed between the LOS and the second most significant MPC. In the LOS and OLOS scenarios, the significant MPCs are within a delay range 40 ns which corresponds to a distance of 12 m. A combination of several factors contributed to this observation. First, a reduction in the dynamic range of the measurement system due to signal loss in the cables rendered the diffuse component indistinguishable from the noise. Secondly, one of the walls behind the Tx antenna was made of plasterboard hence the reflected power is lower. The narrow elevation pattern of the Tx and Rx could have been another factor that resulted in this observation and finally, the higher free space attenuation of mm-wave resulted in a limitation of the propagation distance of the MPCs.
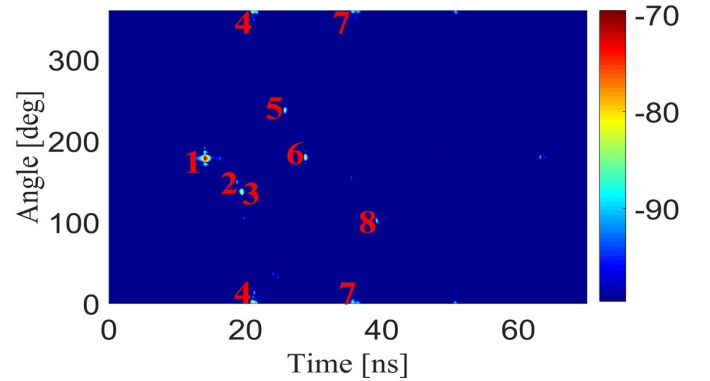

Fig. 4: PADP for the LOS scenario. Color bar units in dB.

A relation of the identified paths and the room geometry is shown in Fig. 6. This relation is obtained by considering the AOA and delay information of the MPCs. Path 6 and 7 are the first and second order reflections of the LOS
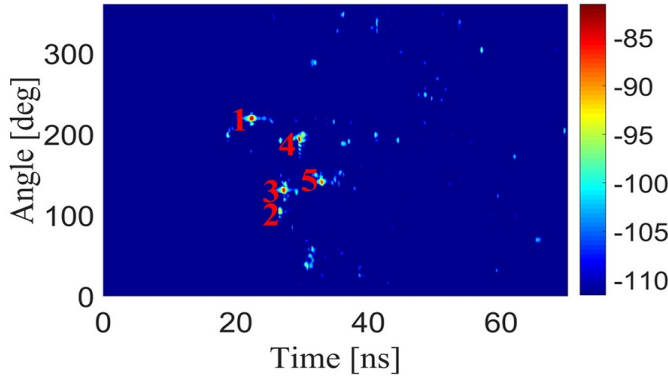
Fig. 5: PADP for the OLOS scenario. Color bar units in dB.

component respectively and are due to the whiteboard shown in Fig. 2. Significant MPCs, path 5 and path 3 are reflections from the concrete wall and the dishwasher, respectively. The plasterboard wall contributes to path 2, which has significantly lower power compared to path 5 from the concrete wall. The path trajectories for the OLOS scenario are shown in Fig. 6 by the dashed line. The first MPC, path 1 is a reflection from the concrete wall in addition to path 5 which is a second order reflection on the concrete wall and the dishwasher. Specular reflection is thus seen to be the dominant propagation mechanism in the mm-wave frequency band in this propagation scenario which is similar to observations made for the mm-wave band centered at 70 GHz in [23].

The elevation angle estimates for the LOS and OLOS are shown in Fig. 7 and Fig. 8 respectively with path labels corresponding to the identified paths in Fig. 4 and Fig. 5. The dominance of the LOS component can be observed in this case too where most power is concentrated on path 1 in Fig. 7. This is observed also in the first order and second order reflected MPCs of the LOS component, path 4 and 7. Path 6 in Fig. 4 which is a first order reflected component of the LOS is not indicated in Fig. 7 since it has an AOA of 180 degrees like the LOS component and therefore cannot be identified in the elevation domain. For the OLOS, the AOA of the significant MPCs are in the azimuth angle range between 100 degrees and 240 degrees as shown in Fig. 8. The lower power of the MPCs resulted in the observed noise components in Fig. 8.

In the LOS and OLOS scenarios, all the paths are in the 90-degree plane. This is as a result of the narrow elevation beam pattern of the antenna which acts as a spatial filter and the fact that the antennas were placed on the same height above the floor. The low resolution in the elevation domain is due to the limited antenna aperture in the z-axis. Despite the low resolution in the elevation domain the UCuA provides un-ambiguous spatial resolution of the channel which is fundamental for the analysis of the multi-user case in section IV-B.

B. Multi-user Scenario

1) Users in LOS condition with different spacing: The spatial-temporal characteristics of the multi-user scenario in the LOS case with different user spacing are shown in Fig.
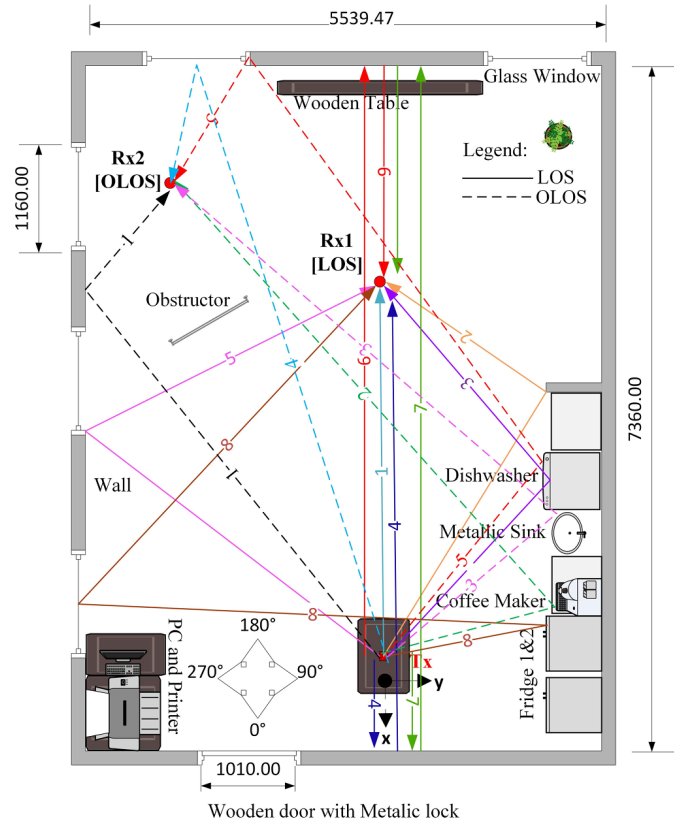

Fig. 6: Trajectory of the MPCs in relation to the room geometry for the LOS and OLOS scenario. The dashed lines represent the MPCs corresponding to the OLOS scenario. Dimensions are in millimeters.
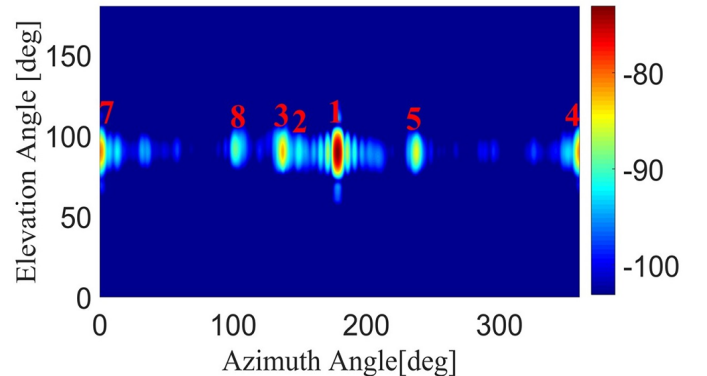

Fig. 7: Elevation and azimuth power angle spectrum for the LOS scenario. Color bar units in dB.

9. The elevation angles are not shown in this analysis since the AOA of the LOS and the MPCs are concentrated on the 90-degree plane as was shown in section IV-A. A relation of the identified paths to the room geometry is shown in Fig. 10. The LOS components for the two users at location A have very similar delay and angle profiles. The MPCs at location A also show a similar trend. This is because the two users share the same scatterers. At location B where user spacing is 0.5 m (50λ at 30 GHz) the LOS components for MS1 and MS2 are separated by about 9 degrees in the spatial domain as shown
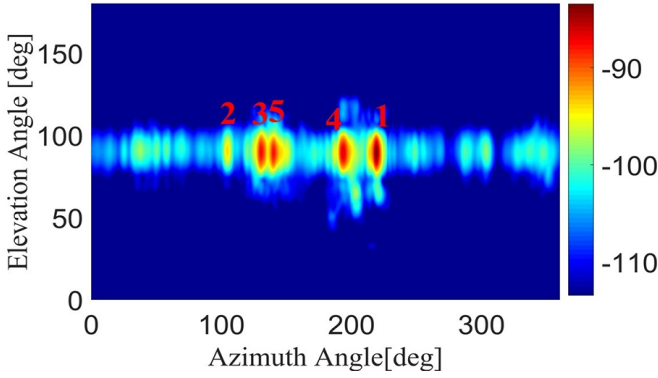
Fig. 8: Elevation and azimuth power angle spectrum for the OLOS scenario. Color bar units in dB.

Fig. 9: Power azimuth delay profile at the four user locations. The users are in LOS conditions. Colour bar units in dB.

by path 1b in Fig. 9. As the user spacing is increased the LOS component for the two users are separated both in spatial and delay domain as shown by path 1d. This is because the distance from the BS to location D is slightly longer compared to the distance to location A.

It can be observed from Fig. 9, that users share the same scatterers at the four locations. The whiteboard is the most significant scatterer as shown by path 5 which is a first order reflection of the LOS component. Path 6, which is a second order reflection of the LOS component is also contributed by the whiteboard and the plasterboard wall behind the Tx. The plasterboard wall, in addition, is the shared scatterer that contributes to the path 3 which is a first order reflection of the LOS component. Path 4 which is a first order reflection, is also from a shared scatterer which is the concrete wall shown in Fig. 10. The ray death for the first order and second order reflection of the LOS component can be seen at location D where the MPCs for path 5 and 6 are not present.

The PAP at the center frequency with ZF-BF is shown in Fig. 11 for the four multi-user locations under LOS conditions. The azimuth angle resolution is limited to the half-space between 90 degrees and 270 degrees as illustrated in Fig. 10 due to the ambiguity of the URA. The field pattern distribution in Fig. 12 is obtained similarly for the half-space between 90 degrees and 270 degrees whose coordinates are given in units of λ at 30 GHz. In this case MS2 is the target user and MS1 the interfering user. The ZF-BF weights for MS2 are used to steer the beams to MS2 and setting nulls in the direction of the interferer MS1.

At location A, where MS1 and MS2 are closely located, the ZF-BF performs fairly well in reducing the interference for the LOS component as demonstrated in Fig. 11a. In addition, the narrow beam pattern due to the higher number of antennas implies that there is improved spatial separation of the users as shown in Fig. 12a. However, at this location, the non-orthogonality of the user channels implies that there is a power penalty due to the transmit power constraint. This can be observable in Fig. 11a where the power of the LOS (path 1a) is reduced almost to the level of the power of the path 2a. The same observation is made in the field pattern shown in Fig. 12a, where the power of the LOS component is lower
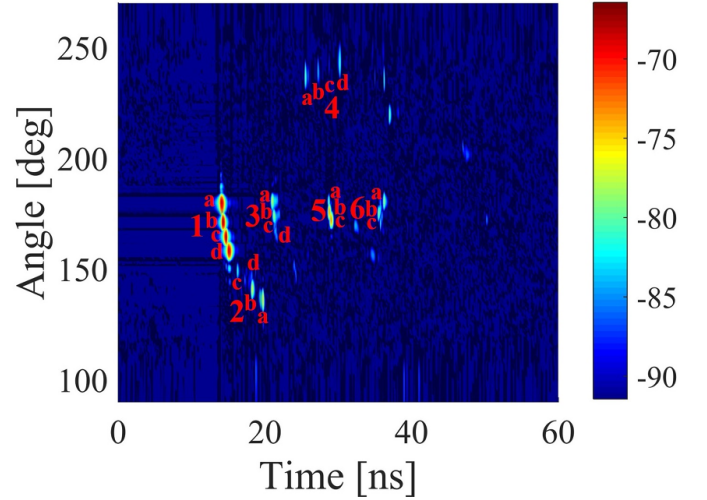
compared to the LOS component at the location B (path 1b), C (path 1c), and D (path 1d) as shown in Fig. 12b, 12c, and 12d respectively.

At location B, the signal power level of the LOS component to MS2 is significantly increased compared to location A as shown in Fig. 12b. This is due to improved user channel orthogonality as a result of the increased user spacing hence the channels are decorrelated thus reducing the power penalty incurred in nulling the interference as compared to when the MSs are placed in location A. At location C, the significant MPCs to MS2 are fewer as shown in Fig. 12c. This is due to the ray death as MS2 is moved further from the significant scatterers like the whiteboard.

The sparsity of the channel as shown in Fig. 4 implies that the degrees of freedom (DoF) is reduced. The DoF is reduced further when the MPCs share scatterers. In this propagation scenario, scatterer sharing can be seen have some detrimental effect on the performance of ZF-BF interference mitigation for the MPCs.

2) Users in LOS and OLOS: In this multi-user scenario, MS2 is the target and MS1 is the interferer. The user channel for MS2 (in an OLOS condition) is highly attenuated relative to the user channel for MS1 (in LOS condition) as outlined in section IV-A. In this case, ZF-BF is used to suppress a strong interferer MS1 and focus the signal energy to the weak targeted user MS2. The field distribution pattern is shown in Fig. 13a. It can be seen that power is steered to the MPCs associated with MS2. The PAP for MS2 in Fig. 13b shows that interference-free communication can be established through paths 1, 2, 4, and 5.

The performance degradation due to user channel similarity is not present in this case. This is because the different location of MS1 and MS2 reduces the number of the common scatterers and thus the DoF is increased. Nulling of the interfering user does not thus result in the power penalty observed in Fig. 12a. This implies the weak user MS2 can have interference-free communication.

(a) Location A.

(b) Location B.

(c) Location C.

(d) Location D.

Fig. 11: PAP with ZF-BF at 28 GHz for MS2 in comparison to the PAP for MS2 and MS1 without ZF-BF. The MPCs labels correspond to paths identified in Fig. 9.
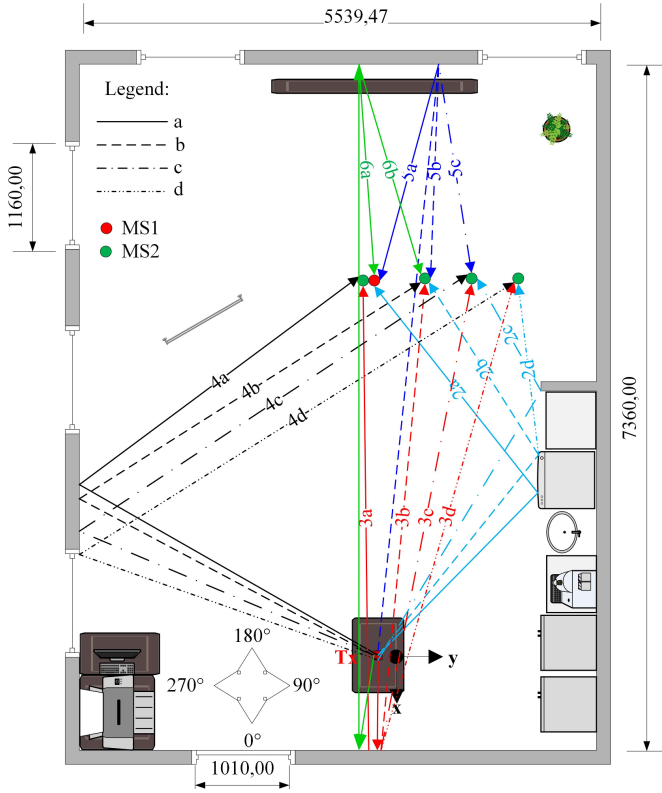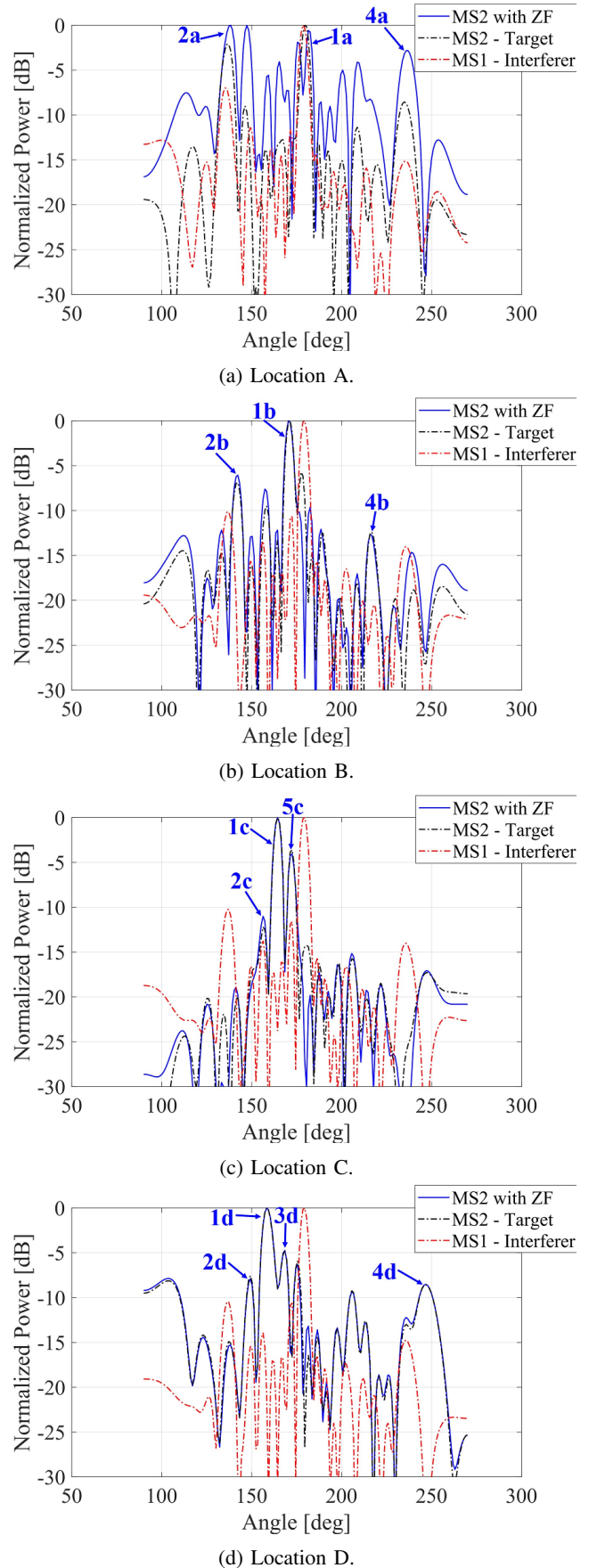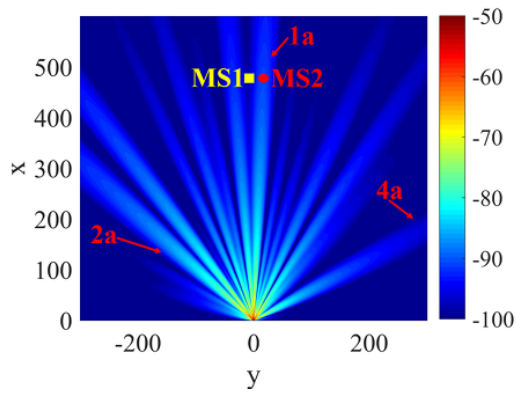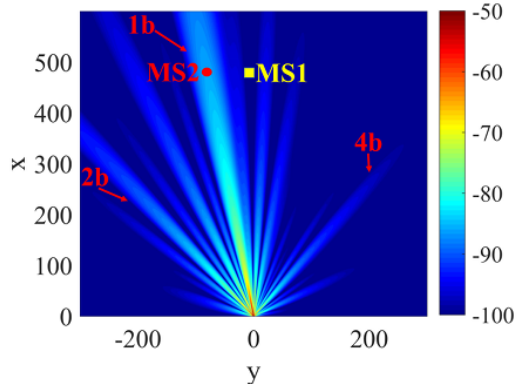

Fig. 10: Trajectory of MPCs in relation to the room geometry for the multi-user scenario in LOS conditions. Propagation paths to each location are represented by different lines as shown in the legend. Dimensions are in millimeters.

V. CONCLUSION

In this paper, high resolution mm-wave channel directional information was obtained using a virtual UCuA. The channel is shown to be sparse with few specular MPCs. Measured multi-user channels using a virtual URA are then analyzed. The effects of the propagation channel impairments on the achievable interference suppression are then demonstrated for critical multi-user scenarios. A large number of BS antennas is shown to be vital in reducing interference from two perspectives: first by simplifying processing at the BS, where nulling is achieved using linear precoding in the downlink at the BS and secondly by focusing the beam to the target user and thus increasing the spatial DoF. When user channels are ill-conditioned, spatial separation is still achievable. However, with a total transmit power constraint, nulling the interference with ZF-BF results in lower signal levels to the targeted user.

(a) MS2 location A.

(b) MS2 location B.
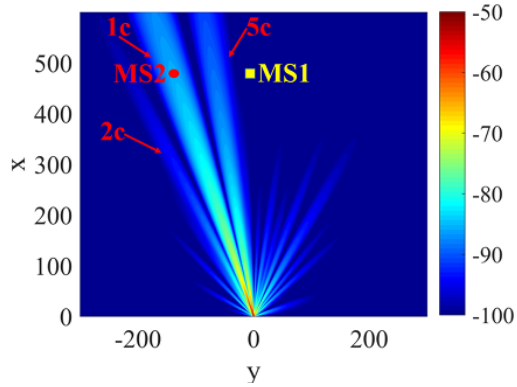
(c) MS2 location C.

(d) MS2 location D.

Fig. 12: Field Pattern Distribution for LOS case. MS2 is the targeted user while MS1 is the interfering user. x and y denote the location coordinates with units λ and the color bar units in dB.

(a) Field pattern distribution with MS2 the target user and MS1 the interfering user. x and y denote the location coordinates with units λ and the colour bar units in dB.
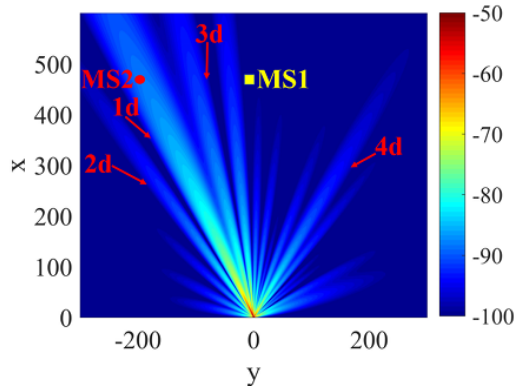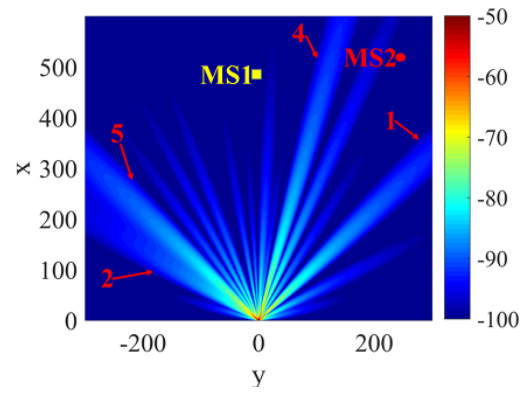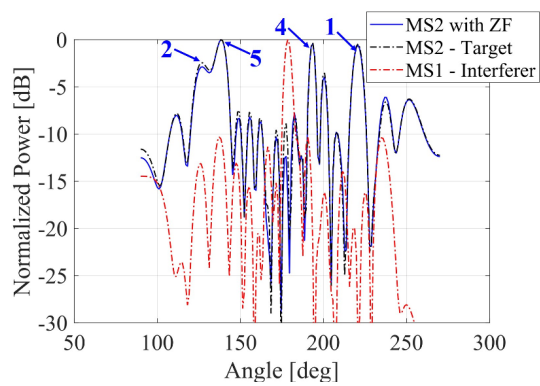

(b) PAP with ZF-BF at 28 GHz for MS2 in comparison to the PAP for MS2 and MS1 without ZF-BF.

Fig. 13: ZF-BF with MS2 as the weak targeted user and MS1 as the strong interferer. The MPCs labels correspond to paths identified in Fig. 5.

REFERENCES

[1] J. G. Andrews, S. Buzzi, W. Choi, S. V. Hanly, A. Lozano, A. C. K. Soong, and J. C. Zhang, "What will 5g be?" *IEEE Journal on Selected Areas in Communications*, vol. 32, no. 6, pp. 1065–1082, June 2014.
[2] W. Roh, J. Y. Seol, J. Park, B. Lee, J. Lee, Y. Kim, J. Cho, K. Cheun, and F. Aryanfar, "Millimeter-wave beamforming as an enabling technology for 5g cellular communications: theoretical feasibility and prototype results," *IEEE Communications Magazine*, vol. 52, no. 2, pp. 106–113, February 2014.
[3] B. Ai, K. Guan, R. He, J. Li, G. Li, D. He, Z. Zhong, and K. M. S. Huq, "On indoor millimeter wave massive mimo channels: Measurement and simulation," *IEEE Journal on Selected Areas in Communications*, vol. 35, no. 7, pp. 1678–1690, July 2017.
[4] G. R. MacCartney and T. S. Rappaport, "A flexible millimeter-wave channel sounder with absolute timing," *IEEE Journal on Selected Areas in Communications*, vol. 35, no. 6, pp. 1402–1418, June 2017.
[5] R. J. Pirkl and G. D. Durgin, "Optimal sliding correlator channel sounder design," *IEEE Transactions on Wireless Communications*, vol. 7, no. 9, pp. 3488–3497, September 2008.
[6] J. Medbo, H. Asplund, J. E. Berg, and N. Jalden, "Directional channel characteristics in elevation and azimuth at an urban macrocell base station," in *2012 6th European Conference on Antennas and Propagation (EUCAP)*, March 2012, pp. 428–432.
[7] J. Hejselbaek, Y. Ji, W. Fan, and G. F. Pedersen, "Channel sounding system for mm-wave bands and characterization of indoor propagation at 28 ghz," *International Journal of Wireless Information Networks*, vol. 24, no. 3, pp. 204–216, Sep 2017. [Online]. Available: https://doi.org/10.1007/s10776-017-0365-0

[8] W. Fan, I. Llorente, J. Nielsen, K. Olesen, and G. Pedersen, "Measured wideband characteristics of indoor channels at centimetric and millimetric bands," *EURASIP Journal on Wireless Communications and Networking*, vol. 2016, no. 58, 2016, special issue on Radio Channel models for higher frequency bands.

[9] S. Ranvier, M. Kyro, K. Haneda, T. Mustonen, C. Icheln, and P. Vainikainen, "Vna-based wideband 60 ghz mimo channel sounder with 3-d arrays," in *2009 IEEE Radio and Wireless Symposium*, Jan 2009, pp. 308–311.

[10] C. Gentile, S. M. Lopez, and A. Kik, "A comprehensive spatial-temporal channel propagation model for the ultra-wideband spectrum 2-8 ghz," in *GLOBECOM 2009 - 2009 IEEE Global Telecommunications Conference*, Nov 2009, pp. 1–6.

[11] F. Zhang, W. Fan, and G. F. Pedersen, "Frequency-invariant uniform circular array for wideband mm-wave channel characterization," *IEEE Antennas and Wireless Propagation Letters*, vol. 16, pp. 641–644, 2017.

[12] J. Medbo, H. Asplund, and J. E. Berg, "60 ghz channel directional characterization using extreme size virtual antenna array," in *2015 IEEE 26th Annual International Symposium on Personal, Indoor, and Mobile Radio Communications (PIMRC)*, Aug 2015, pp. 176–180.

[13] J. Medbo, N. Seifi, and H. Asplund, "Frequency dependency of measured highly resolved directional propagation channel characteristics," in *European Wireless 2016; 22th European Wireless Conference*, May 2016, pp. 1–6.

[14] J. Medbo, K. Brner, K. Haneda, V. Hovinen, T. Imai, J. Jrvelainen, T. Jms, A. Karttunen, K. Kusume, J. Kyrlinen, P. Kysti, J. Meinil, V. Nurmela, L. Raschkowski, A. Roivainen, and J. Ylitalo, "Channel modelling for the fifth generation mobile communications," in *The 8th European Conference on Antennas and Propagation (EuCAP 2014)*, April 2014, pp. 219–223.

[15] K. Guan, G. Li, T. Krner, A. F. Molisch, B. Peng, R. He, B. Hui, J. Kim, and Z. Zhong, "On millimeter wave and thz mobile radio channel for smart rail mobility," *IEEE Transactions on Vehicular Technology*, vol. 66, no. 7, pp. 5658–5674, July 2017.

[16] X. Gao, O. Edfors, F. Rusek, and F. Tufvesson, "Massive mimo performance evaluation based on measured propagation data," *IEEE Transactions on Wireless Communications*, vol. 14, no. 7, pp. 3899–3911, July 2015.

[17] J. Flordelis, X. Gao, G. Dahman, F. Rusek, O. Edfors, and F. Tufvesson, "Spatial separation of closely-spaced users in measured massive multi-user mimo channels," in *2015 IEEE International Conference on Communications (ICC)*, June 2015, pp. 1441–1446.

[18] R. He, B. Ai, G. L. Stuber, G. Wang, and D. Z. Zhong, "Geometrical based modeling for millimeter wave mimo mobile-to-mobile channels," *IEEE Transactions on Vehicular Technology*, vol. PP, no. 99, pp. 1–1, 2017.

[19] S. S. Zhekov, A. Tatomirescu, and G. F. Pedersen, "Antenna for ultra-wideband channel sounding," *IEEE Antennas and Wireless Propagation Letters*, vol. 16, pp. 692–695, 2017.

[20] A. Wiesel, Y. C. Eldar, and S. Shamai, "Zero-forcing precoding and generalized inverses," *IEEE Transactions on Signal Processing*, vol. 56, no. 9, pp. 4409–4418, Sept 2008.

[21] E. G. Larsson, O. Edfors, F. Tufvesson, and T. L. Marzetta, "Massive mimo for next generation wireless systems," *IEEE Communications Magazine*, vol. 52, no. 2, pp. 186–195, February 2014.

[22] Q. H. Spencer, C. B. Peel, A. L. Swindlehurst, and M. Haardt, "An introduction to the multi-user mimo downlink," *IEEE Communications Magazine*, vol. 42, no. 10, pp. 60–67, Oct 2004.

[23] K. Haneda, J. Jrvelinen, A. Karttunen, M. Kyr, and J. Putkonen, "Indoor short-range radio propagation measurements at 60 and 70 ghz," in *The 8th European Conference on Antennas and Propagation (EuCAP 2014)*, April 2014, pp. 634–638.

Allan Wainaina Mbugua received his B.Sc. Telecommunication and Information Engineering from Jomo Kenyatta University of Agriculture and Technology, Kenya in 2014. He is currently pursuing M.Sc. Telecommunications Engineering at the University of Cassino and Southern Lazio, Italy. From February 2017 to June 2017, he was an Erasmus guest student in M.Sc. Wireless Communication Systems, Alborg University. Since September 2017, he has been a research Intern with the Antennas, Propagation and Millimetre-Wave Systems Section, Aalborg University. The focus of his work is on millimeter-wave radio channel measurements and channel characterization.
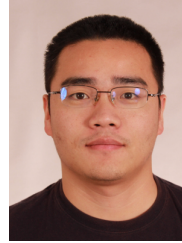
Wei Fan received his Bachelor of Engineering degree from Harbin Institute of technology, China in 2009, Master's double degree with highest honours from Politecnico di Torino, Italy and Grenoble Institute of Technology, France in 2011, and Ph.D. degree from Aalborg University, Denmark in 2014. From February 2011 to August 2011, he was with Intel Mobile Communications, Denmark as a research intern. He conducted a three-month internship at Anite telecoms oy, Finland in 2014. His main areas of research are over the air testing of multiple antenna systems, radio channel sounding, modeling and emulation. He is currently an associate professor at the Antennas, Propagation and Millimeter-wave Systems (APMS) Section at Aalborg University.
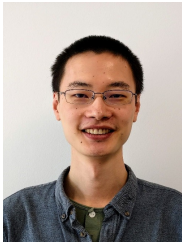
Yilin Ji received his Bachelor and Master degree in Wireless Communications from Tongji University, China in 2013 and 2016, respectively. He is currently a Ph.D. Fellow at the section of Antennas, Propagation and Millimeter-wave Systems (APMS) at Aalborg University. The focus of his work is mainly on antenna array signal processing, channel characterization, and OTA testing.

Gert Frølund Pedersen was born in 1965 and married to Henriette and have 7 children. He received the B.Sc. E.E. degree, with honour, in electrical engineering from College of Technology in Dublin, Ireland in 1991, and the M.Sc. E.E. degree and Ph.D. from Aalborg University in 1993 and 2003. He has been with Aalborg University since 1993 where he is a full Professor heading the Antenna, Propagation and Networking LAB with 36 researcher. Further he is also the head of the doctoral school on wireless communication with some 100 phd students enrolled. His research has focused on radio communication for mobile terminals especially small Antennas, Diversity systems, Propagation and Biological effects and he has published more than 175 peer reviewed papers and holds 28 patents. He has also worked as consultant for developments of more than 100 antennas for mobile terminals including the first internal antenna for mobile phones in 1994 with lowest SAR, first internal triple-band antenna in 1998 with low SAR and high TRP and TIS, and lately various multi antenna systems rated as the most efficient on the market. He has worked most of the time with joint university and industry projects and have received more than 12 M\$ in direct research funding. Latest he is the project leader of the SAFE project with a total budget of 8 M\$ investigating tunable front end including tunable antennas for the future multiband mobile phones. He has been one of the pioneers in establishing Over-The-Air (OTA) measurement systems. The measurement technique is now well established for mobile terminals with single antennas and he was chairing the various COST groups (swg2.2 of COST 259, 273, 2100 and now ICT1004) with liaison to 3GPP for over-the-air test of MIMO terminals. Presently he is deeply involved in MIMO OTA measurement.